Bone Reports 19 (2023) 101713

Contents lists available at ScienceDirect

Bone Reports

journal homepage: www.elsevier.com/locate/bonr

Relationship between bone marrow adipose tissue and kidney function in postmenopausal women

Sammy Badr [a], Anne Cotten [a], Romuald Mentaverri [b], Daniela Lombardo [c], Julien Labreuche [d], Claire Martin [d], Lucie Hénaut [b], Bernard Cortet [c], Julien Paccou [c,*]

[a] Univ. Lille, CHU Lille, MABlab ULR 4490, Department of Radiology and Musculoskeletal Imaging, F-59000 Lille, France
[b] UR UPJV 7517, Pathophysiological Mechanisms and Consequences of Cardiovascular Calcifications (MP3CV), Picardie Jules Verne University, 80025 Amiens, France
[c] Univ. Lille, CHU Lille, MABlab ULR 4490, Department of Rheumatology, F-59000 Lille, France
[d] CHU Lille, Department of Biostatistics, F-59000 Lille, France

ARTICLE INFO

Keywords:
Bone marrow adipose tissue
Chronic kidney disease
Estimated glomerular filtration rate
Bone mineral density
Osteoporosis

ABSTRACT

Introduction: Bone marrow adipose tissue (BMAT) is associated with aging, osteoporosis, and chronic kidney disease (CKD). To date, the association between BMAT and kidney function in postmenopausal women has not been thoroughly investigated. The main purpose of this study was to determine whether a relationship exists between proton density fat fraction (PDFF) and kidney function in postmenopausal women.

Methods: We investigated the cross-sectional association between estimated glomerular filtration rate (eGFR) – calculated using the Chronic Kidney Disease Epidemiology Collaboration (CKD-EPI) equation – and PDFF – measured at the lumbar spine and proximal femur using Water Fat Imaging (WFI) MRI – in 199 postmenopausal women from the ADIMOS cohort study. We also performed DXA scans and laboratory measurements of sclerostin and c-terminal Fibroblast Growth Factor 23 (cFGF23).

Results: Participants' mean age was 67.5 (standard deviation, SD 10.0) years. Their median eGFR was 85.0 (interquartile range, IQR 72.2–95.0) ml/min/1.73 cm^2, and their mean lumbar spine PDFF was 57.9 % (SD 9.6). When classified by eGFR-based CKD stages, 41.7 % of the cohort had an eGFR $\geq$ 90 ($n = 83$), 47.2 % had an eGFR of 60–89.9 ($n = 94$), and 11.1 % had an eGFR of 30–59.9 ($n = 22$). Participants with eGFR $\geq$ 90 had a lower lumbar spine PDFF than those with eGFR 60–89.9 (mean 55.8 % (9.8) vs. 58.9 % (9.0), $p = 0.031$) and those with eGFR 30–59.9 (55.8 % (9.8) vs. 60.8 % (9.8), $p = 0.043$). However, the differences did not remain significant after adjusting for predetermined confounders, including age, diabetes, Charlson comorbidity index, recent history of fragility fracture, appendicular lean mass, and lumbar spine BMD. The inclusion of sclerostin and/or cFGF23 as suspected mediators did not alter the findings. When proximal hip imaging-based PDFF was considered, no significant differences were found between the eGFR categories in the unadjusted and adjusted analyses.

Conclusion: No evidence of an association between kidney function and bone marrow adiposity was found either in the lumbar spine or proximal femur in a cohort of postmenopausal women.

1. Introduction

The connection between bone marrow adipose tissue (BMAT) and bone metabolism has emerged as an exciting area of research (Lecka-Czernik et al., 2018; Paccou et al., 2019). This was made possible by the development of BMAT imaging using Magnetic Resonance Imaging (MRI), which is still considered the gold standard (Karampinos et al., 2018; Ruschke and Karampinos, 2022). BMAT can be quantified noninvasively in vivo by determining the proton density fat fraction (PDFF) as a %. Findings on the associations are consistent, particularly for bone mineral density (BMD) assessed using dual-energy X-ray absorptiometry (DXA). Cross-sectional studies have shown that higher PDFF is associated with lower BMD (Paccou et al., 2015; Li et al., 2020). However, the exact role of BMAT in bone health and its relationship with fragility fractures remains unresolved (Beekman et al., 2023; Schwartz et al., 2013; Woods et al., 2022). Moreover, factors associated with this

* Corresponding author at: Department of Rheumatology, Lille University Hospital, Lille, France.
E-mail address: julien.paccou@chru-lille.fr (J. Paccou).

https://doi.org/10.1016/j.bonr.2023.101713
Received 11 June 2023; Received in revised form 8 August 2023; Accepted 3 September 2023

relationship remain largely unidentified, even though Fibroblast Growth Factor 23 (FGF23) and sclerostin – both secreted by osteocytes – might influence marrow adipogenesis (Courtalin et al., 2023; Fairfield et al., 2018; Li et al., 2013).

Further understanding of the mechanisms underlying this association could lead to better diagnosis and treatment of osteoporosis. This might be of particular significance in populations of individuals with metabolic diseases (e.g., diabetes) and chronic kidney disease (CKD), in which BMAT abnormalities have been demonstrated (Moorthi et al., 2015; Wang et al., 2022a; Hernandez et al., 2018a; Woods et al., 2018). In a small sample size study conducted in 2015, Moorthi et al. found that patients with CKD (n = 8, mean estimated glomerular filtration rate (eGFR) = 24 ml/min/1.73 cm^2) had higher lumbar spine PDFFs than healthy adults matched for race, sex, and age (Moorthi et al., 2015). A few years later, Woods et al. reported that participants with an estimated glomerular filtration rate (eGFR) <45 ml/min/1.73 cm^2 had higher lumbar spine PDFFs than those with eGFR>60 in the AGES-Reykjavik cohort (Woods et al., 2018). Further investigation is necessary to validate these findings in CKD and to evaluate whether PDFF is associated with kidney function. It is important to note that previous studies were limited in that the number of participants was small (Moorthi et al., 2015), women and men of all ages were included (Woods et al., 2018), no adjustments were made for fracture status or lumbar spine areal BMD values (Moorthi et al., 2015; Woods et al., 2018), and BMAT at the proximal femur was not investigated. Furthermore, sclerostin and FGF23 circulate at elevated levels in CKD, and elevated sclerostin and FGF23 levels might be associated with higher PDFFs (Pelletier et al., 2013; Mazzaferro et al., 2018; Desbiens et al., 2022).

We conducted this cross-sectional study using data from the ADIMOS cohort (Paccou et al., 2023) to determine whether a relationship exists between PDFF and kidney function in postmenopausal women aged 50 years and older, and whether sclerostin or FGF23 might mediate this relationship.

2. Patient and methods

2.1. Participants

The ADIMOS study is a case-control study (Clinical Gov NCT03219125) designed to examine the relationship between imaging-based PDFF and fragility fractures in postmenopausal women, at both the lumbar spine and proximal femur (Paccou et al., 2023). The cases were postmenopausal women with recent fragility fractures (<12 months old), and the controls were postmenopausal women with osteoarthritis and no history of fragility fractures. Chronic kidney disease with calculated creatinine clearance <30 ml/mn/1.73 cm^2 was an exclusion criterion, as were contraindications to MRI. Among the exclusion criteria, there was a current use of compounds known to affect BMAT – including glucocorticoids, osteoporosis medications (bisphosphonates, raloxifene, calcitonin, or teriparatide), thiazolidinediones, and estrogen therapy. Prior use of osteoporosis and estrogen therapy treatments over 12 months old was allowed.

This ancillary study (the ADIMOS-eGFR study) was approved by the local Institutional Review Board. All participants provided their written informed consent.

2.2. Imaging-based proton density fat fraction

MRI examinations were performed on a 3-T full-body scanner (Ingenia; Philips Medical Systems, Best, The Netherlands) using a built-in 12-channel posterior body coil and a 16-channel anterior coil. The patients were placed in the supine position and introduced head-first into the tunnel. The imaging protocol was supervised by a senior musculoskeletal radiologist and comprised a conventional exploration of the lumbar spine (morphological assessment) and optimized chemical shift encoding-based water-fat imaging sequences (mDixon-Quant; Philips Healthcare, Best, The Netherlands) at the lumbar spine and non-dominant hip (BMAT quantification). Based on these latter acquisitions, PDFF maps were computed offline using a pre-calibrated seven-peak fat spectrum and a single T2*correction. The protocol for acquiring MRI images to determine PDFF did not need gadolinium contrast administration.

MRI segmentation was performed on a dedicated workstation using an IntelliSpace Portal (Philips Healthcare, Best, Netherlands). The three most central slices of the computed maps were chosen, and a polygonal region of interest (ROI) was drawn on the vertebral body from L1 to L4, excluding fractured vertebrae, immediate subchondral bone, bone marrow-replacing lesions, severe degenerative changes, and basivertebral veins. Subsequently, the mean PDFF value at the lumbar spine was obtained for each participant as an average of the L1–L4 segmented vertebrae (Fig. 1). Similarly, the mean PDFF value at the nondominant hip was obtained by drawing an ROI on the femoral head, femoral neck, and proximal femoral shaft (Fig. 2).

A more detailed description of the imaging protocol and previously obtained correlations were reported in the leading publication of the ADIMOS study (Paccou et al., 2023).

2.3. Kidney function

Serum creatinine was measured from fasting blood samples obtained at the time of PDFF evaluation. The estimated glomerular filtration rate (eGFR) was calculated using the Chronic Kidney Disease Epidemiology Collaboration equation. For analyses, participants were stratified by eGFR-based CKD stages i.e. eGFR ≥90 ml/mn/1.73 cm^2, eGFR 60–89.9 ml/mn/1.73 cm^2, and eGFR 30–59.9 ml/mn/1.73 cm^2.

2.4. Sclerostin

ELISA kits were purchased from TECO Medical (Sissach, Switzerland) (Human Sclerostin EIA, High Sensitivity). Serum samples were analyzed and sclerostin concentrations were measured according to the manufacturer's instructions. Samples were run in duplicate, with an average coefficient of variation (CV) of 2.5 % between runs for sclerostin. Concentrations with high CV percentages (>10 %) were excluded from analysis.

2.5. FGF23

C-terminal FGF23 was measured using a second-generation C-terminal ELISA kit from Immutopics (San Clemente, CA, USA), according to the manufacturer's instructions. The laboratory intra-assay coefficients of variation were 3.4 % and 2.4 % at 36 and 217 relative units (RU)/ml, respectively. The interassay coefficient of variation was <6 %. The limit of detection was 1.5 RU/ml.

2.6. Other measurements

Osteoporosis risk factors such as current smoking, excessive alcohol consumption, and previous use of oral corticosteroids were collected. The Charlson Comorbidity Index (CCI), leisure time activity (score 0–15), and medication data were recorded.

Bone mineral density (BMD) was measured at the lumbar spine (L1–L4) and non-dominant hip using DXA (HOLOGIC Discovery A S/N 81360). Data included BMD (in g/cm^2 of hydroxyapatite) at three sites: the lumbar spine, total hip, and femoral neck. As recommended by the WHO, osteoporosis was defined as a T-score ≤ −2.5.

Whole-body DXA scans were performed to evaluate body composition. The data included appendicular lean mass (aLM, kg), total body fat (TBF, kg), and visceral adipose tissue (VAT, cm^2). The aLM was defined as the sum of the lean soft tissue masses of the four limbs.

Fasting blood samples were collected from all patients. Total calcium, phosphorus, and high-sensitivity C-reactive protein (hs-CRP)

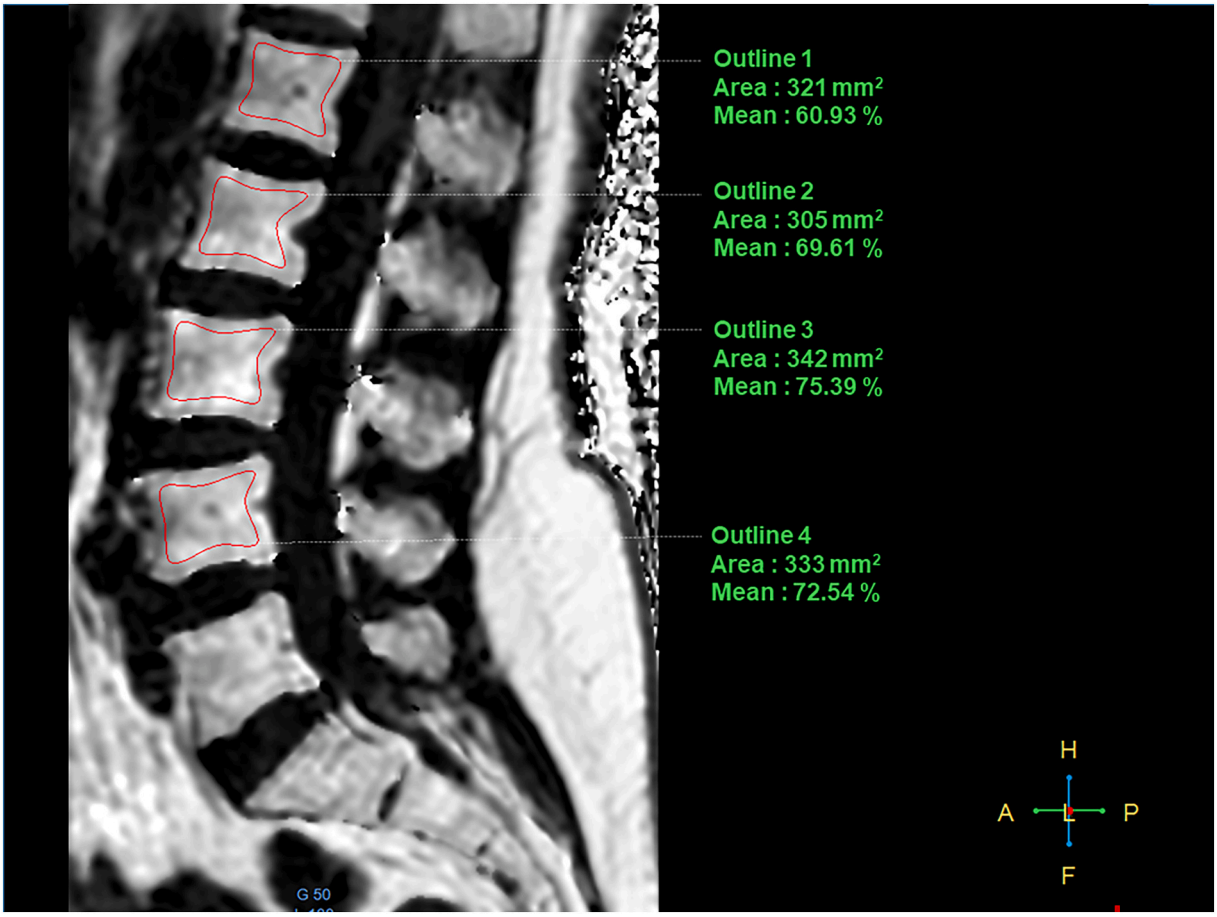

Fig. 1. PDFF map of the lumbar spine computed from a multi-echo gradient echo sequence (mDixon-Quant) acquired in the sagittal plane in a 63-year old postmenopausal woman. The region of interest (green) was placed on the L1–L4 vertebral bodies. The mean PDFF value for this participant was calculated as the average of the L1–L4 segmented vertebrae measurements.

levels were assessed using routine assays. Parathormone (PTH) was measured by chemiluminescent immunoassay using an automatic analyzer (Architect, Abbott Laboratories, USA). 25-OH vitamin D was measured by competitive chemiluminescent immunoassay using an IDS-iSYS device (IDS, Pouilly en auxois, France). Procollagen I intact N-terminal (PINP) and serum cross laps (CTX) were measured by chemiluminescence assay using the IDS-iSYS Multi-Discipline Automated Analyzer (Immunodiagnostic Systems, Inc., Fountain Hills, AZ, USA).

2.7. Statistical analyses

Categorical variables were reported as frequencies (percentages). Quantitative variables were reported as mean (standard deviation, SD) in the case of normal distributions, or median (interquartile range, IQR). The normality of distributions was assessed using histograms and the Shapiro-Wilk test.

Patient characteristics at baseline were described and compared between the three eGFR-based CKD stage groups using the chi-square test (or Fisher's exact test when the expected cell frequency was <5) for categorical variables, and one-way analysis of variance (ANOVA) (or Kruskal-Wallis test in case of non-normal distribution) for quantitative variables.

Comparisons of PDFFs measurements between the eGFR-based CKD stage groups were further investigated after adjustments for predefined confounding factors (age, diabetes, CCI, recent fragility fractures, aLM, lumbar spine BMD (hip BMD), cFGF23, and sclerostin) using analysis covariance (ANCOVA) models. The association of predefined confounding factors with PDFFs is reported in Supplemental Table 1. We derived from the ANCOVA model the adjusted means of PDFFs in each eGFR group with their 95 % confidence intervals. Primary analyses were performed by treating eGFR as 3-level variable according to the established CKD stages. We further analyzed eGFR as a continuous variable using linear regression models to estimate the change in PDFFs per 10 % increase in eGFR (expressed as regression coefficients with their 95 % confidence intervals). For ANCOVA and linear models, the normality and homoscedasticity of the residuals were checked.

All statistical tests were performed at a two-tailed α-level of 0.05 using SAS software (version 9.4; SAS Institute, Cary, NC, USA).

3. Results

3.1. Baseline characteristics

Table 1 shows the baseline characteristics of the 199 postmenopausal women. Participants had a mean age of 67.5 (SD 10.0) years, median eGFR of 85.0 (IQR 72.2–95.0) ml/min/1.73 cm^2, and mean lumbar spine PDFF of 57.9 % (SD 9.6). When classified by eGFR category, 41.7 % of the cohort had an eGFR ≥90 (median 96.0 (IQR 93.0–99.0) ml/mn/1.73 cm^2), 47.2 % had an eGFR of 60–89.9 (median 78.0 (IQR 71.0–83.0) ml/mn/1.73 cm^2), and 11.1 % had an eGFR of 30–59.9 (median 52.5 (IQR 41.3–56.0) ml/mn/1.73 cm^2).

Participants with lower eGFRs were significantly older and had a higher prevalence of diabetes, higher CCIs, and higher cFGF23 levels (all $p < 0.05$). In the lowest eGFR group, a trend towards higher levels of serum sclerostin was also observed, with p-values close to the significance level of 0.05 ($p = 0.090$ for the comparison with the intermediate

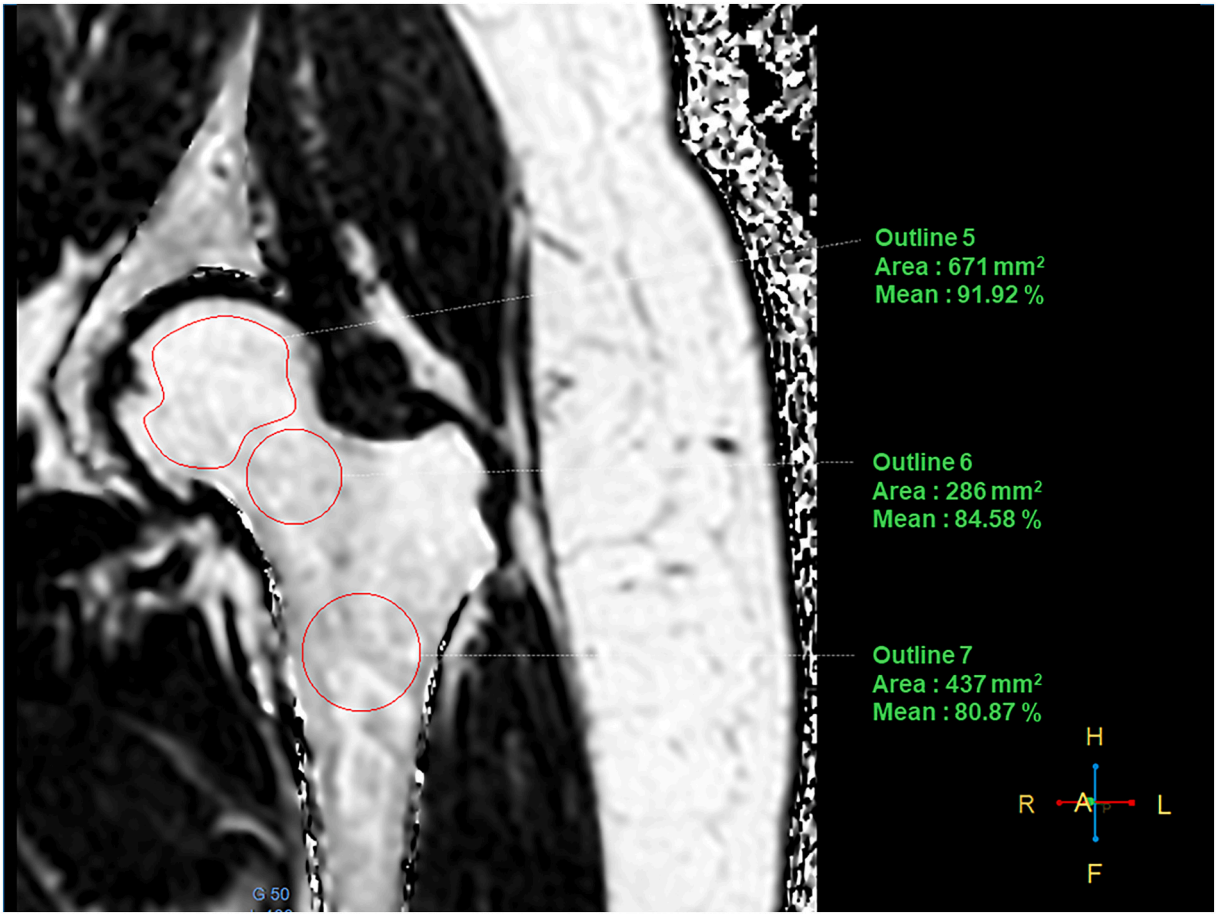

Fig. 2. PDFF map of the non-dominant hip computed from a multi-echo gradient echo sequence (mDixon-Quant) acquired in the coronal plane (same patient as Fig. 1).

group, and $p = 0.054$ for the comparison with the highest group). No differences in bone turnover markers (CTX and PINP), aLM, or BMD were observed across the eGFR groups.

When classified by eGFR category, participants with eGFR ≥90 had lower lumbar spine PDFFs than those with eGFR 60–89.9 (mean (SD) 55.8 % (9.8) vs. 58.9 % (9.0), $p = 0.031$) and those with eGFR 30–59.9 (55.8 % (9.8) versus 60.8 % (9.8), $p = 0.043$). When proximal hip imaging-based PDFFs were considered, no significant differences in femoral neck or diaphysis PDFFs were found across the eGFR groups.

Comparison of lumbar spine and proximal hip imaging-based PDFF by eGFR category.

When imaging-based PDFFs were compared, the association disappeared when adjusted only for age (model 1). No significant differences between the eGFR categories were found in model 2 after adjusting for other predetermined confounders, including age, diabetes, CCI, recent fragility fractures, aLM, and lumbar spine BMD (or hip BMD) (Table 2).

The inclusion of cFGF23 (model 3) and finally sclerostin (model 4) as suspected mediators had no impact on imaging-based PDFF comparisons across the kidney function categories.

Furthermore, investigating the BMAT relationships by treating eGFR as a continuous variable to increase the power of the analysis did not change the results before and after adjusting for predetermined confounders (Table 2).

4. Discussion

In this study, imaging-based PDFFs at the lumbar spine and proximal hip were compared across eGFR categories (≥90, 60–89.9, and 30–59.9 ml/mn/1.73 cm^2) in a cohort of postmenopausal women aged 50 to 90 years old. After adjusting for predetermined confounding factors, the results showed comparable PDFFs, regardless of the measurement site. The inclusion of sclerostin or cFGF23 as suspected mediators of BMAT and kidney function did not change the findings.

To date, only a few studies have investigated the association between BMAT and kidney function. Moorthi et al. (Moorthi et al., 2015) demonstrated that the percentage of bone marrow adiposity – quantified using the ^{1}H-MRS technique – was higher in the lumbar spine of patients with moderate to late stage CKD ($n = 8$ (5 women), mean age 59.8 ± 7.2 years, and mean eGFR 24 ± 8 ml/min/1.73 m^2) compared to patients with normal kidney function (n = 8, mean age 58.1 ± 10.2 years) matched for race, gender, and age. Mean bone marrow adiposity at L2 was 57.8 ± 12.2 % in subjects with CKD versus 41.7 ± 10.8 % in controls ($p = 0.02$). At L3, mean bone marrow adiposity was 56.9 ± 11.1 % in the CKD group versus 44.8 ± 11.4 % in the control group (p = 0.02). Similarly, at L4, mean bone marrow adiposity was 59.8 ± 10.1 % versus 46.3 ± 11.6 % ($p = 0.03$). Among the limitations of that study are the small sample size and the fact that no BMD or fracture assessments were performed. In a subsequent study, Woods et al. (Woods et al., 2018) investigated the association between eGFR and ^{1}H-MRS-quantified lumbar spine marrow adiposity in adults in the AGES-Reykjavik study. A comparison was performed between subjects with eGFR >60 ($n = 297$) and those with eGFR 45–60 ($n = 120$) or eGFR <45 ($n = 58$). After adjusting for age, sex, diabetes, and visceral adiposity, marrow adiposity (L1–L4) was higher in patients with eGFR <45 (adjusted mean: 58.5 %; 95 % CI: 56.2–60.7) than in those with eGFR>60 (adjusted mean: 53.8 %; 95 % CI: 52.8–54.8) ($p = 0.0002$). However, marrow adiposity values in patients with eGFR 45–60 and patients with eGFR>60 were

Table 1
Patients' general characteristics and biochemistry results at baseline.

	N	eGFR 30 to 59.9 ($n = 22$)	N	eGFR 60 to 89.9 (n = 94)	N	eGFR ≥ 90 (n = 83)	p-Value
Age [years]	22	75.95 ± 10.43	94	69.09 ± 10.52	83	63.36 ± 6.91	**<0.001**
Height [cm]	22	160.4 ± 9.78	94	160.8 ± 5.80	83	159.4 ± 6.38	0.31
Weight [kg]	22	75.36 ± 19.52	94	69.83 ± 16.17	83	67.93 ± 14.08	0.14
BMI [kg/m^2]	22	29.0 ± 5.8	94	27.0 ± 6.2	83	26.8 ± 5.4	0.27
Leisure time activity (score 0–15)	20[a]	8.2 ± 2.8	94	9.1 ± 2.6	82[a]	9.1 ± 2.4	0.27
Comorbidities							
Non-metastatic cancer	22	6 (27.3)	94	18 (19.1)	83	14 (16.9)	0.54
Type 2 diabetes	22	7 (31.8)	94	11 (11.7)	83	6 (7.2)	**0.007**
Chronic pulmonary disease	22	1 (4.5)	94	6 (6.4)	83	7 (8.4)	0.77
Stroke or TIA	22	2 (9.1)	94	6 (6.4)	83	3 (3.6)	0.40
Charlson Comorbidity Index	22	6 (4 to 6)	94	3 (2 to 4)	83	2 (0 to 3)	**<0.001**
Clinical risk factors							
Imminent fracture	22	16 (72.7)	94	47 (50.0)	83	37 (44.6)	0.063
Excessive alcohol consumption	22	1 (4.5)	94	6 (6.4)	83	5 (6.0)	0.95
Current smoking	22	0 (0)	94	11 (11.7)	83	12 (14.5)	0.17
Family history of hip fracture	22	3 (13.6)	94	8 (8.5)	83	11 (13.3)	0.56
Previous use of corticosteroids	22	3 (13.6)	94	4 (4.3)	83	3 (3.6)	0.18
Biochemistry results							
Hs-CRP [mg/l]	22	4.0 (3.0 to 12.0)	94	3.0 (3.0 to 7.0)	83	3.0 (3.0 to 4.0)	**0.039**
HBA1C [%]	22	5.9 (5.5 to 6.4)	93[b]	5.5 (5.4 to 5.9)	83	5.5 (5.3 to 5.7)	**0.011**
Phosphorus [mmol/l]	22	1.1 ± 0.2	93[b]	1.1 ± 0.2	83	1.1 ± 0.1	0.13
Calcium [mmol/l]	22	2.4 ± 0.1	94	2.4 ± 0.1	83	2.4 ± 0.1	0.39
25(OH) vitamin D [ng/ml]	22	29.0 ± 11.4	94	26.6 ± 10.9	83	29.9 ± 12.2	0.16
Serum PTH [pg/ml]	22	53.5 (36.0 to 65.0)	94	45.0 (36.0 to 57.0)	83	42.0 (31.0 to 55.0)	0.17
Creatinine [μmol/l]	22	88.0 (88.0 to 106.0)	94	71.0 (62.0 to 71.0)	83	53.0 (53.0 to 62.0)	**<0.001**
Creatinine clearance (CKD-EPI) [ml/mn]	22	52.5 (41.3 to 56.0)	94	78.0 (71.0 to 83.0)	83	96.0 (93.0 to 99.0)	**<0.001**
Biochemical markers of bone							
PINP [ng/ml]	22	41.5 (33.0 to 97.0)	88[c]	63.5 (46.0 to 78.5)	82[c]	63.5 (48.0 to 78.0)	0.15
CTX [pmol/l]	21[b]	2108 (1799 to 4820)	94	3344 (2256 to 4884)	83	3350 (2408 to 4698)	0.29
SOST	22	0.84 ± 0.34	93[d]	0.67 ± 0.17	83	0.65 ± 0.18	**0.048**
cFGF23	22	158.9 (93.8 to 242.8)	93[d]	89.96 (69.9 to 122.4)	83	77.09 (57.6 to 110.2)	**<0.001**
Bone mineral density							
BMD lumbar spine (g/cm^2)	21[e]	0.959 ± 0.215	94	0.901 ± 0.175	83	0.867 ± 0.166	0.082
BMD total hip (g/cm^2)	21[f]	0.808 ± 0.181	92[f]	0.810 ± 0.153	83	0.815 ± 0.139	0.96
BMD femoral neck (g/cm^2)	21[f]	0.651 ± 0.132	92[f]	0.677 ± 0.133	83	0.689 ± 0.133	0.49
Body composition							
Total body fat (kg)	20[g]	33.1 ± 12.6	93[g]	31.3 ± 11.4	81[g]	30.3 ± 10.0	0.57
Visceral adipose tissue (cm^2)	20[g]	194.2 ± 108.3	93[g]	160.7 ± 81.9	81[g]	139.7 ± 70.1	**0.047**
Appendicular lean mass (kg)	20[g]	14.2 ± 3.5	93[g]	13.7 ± 2.6	81[g]	13.1 ± 2.3	0.14
Fat content (imaging-based)							
PDFF lumbar spine (%)	22	60.8 ± 9.8	94	58.9 ± 9.0	83	55.8 ± 9.8	**0.030**
PDFF femoral neck (%)	21[h]	81.8 ± 9.2	89[h]	82.8 ± 8.2	82[h]	80.9 ± 8.2	0.34
PDFF femoral diaphysis (%)	21[h]	80.6 ± 8.3	89[h]	81.2 ± 9.9	82[h]	79.9 ± 8.7	0.64

Values are expressed as numbers (%), mean ± SD or mean [95 % CI] or median (IQR). Statistically significant results are indicated in bold type.
Abbreviations: SD = Standard Deviation; IQR = Interquartile Range; PTH = parathyroid hormone; PINP = procollagen type 1 N-terminal propeptide; CTX = collagen type 1 cross-linked C-telopeptide; hs-CRP = high-sensitivity C-reactive protein; TIA: transient ischemic attack; BMD: bone mineral density; PDFF: proton density fat fraction; CI = Confidence Interval.

[a] Leisure time activity scores were not available in 3 patients.
[b] HBA1C, CTX and phosphorus measurements were not available for each in 1 patient.
[c] PINP measurement was not available in 7 patients (unacceptable quantity of serum).
[d] Serum sclerostin and cFGF23 measurements were not available in 1 patient (unacceptable quantity of serum).
[e] Lumbar spine BMD measurement was not performed in 1 patient (vertebral fractures at L1, L2, L3).
[f] Hip BMD measurements were not available in 3 patients (bilateral hip arthroplasty).
[g] Body composition measurements were not performed in 5 patients (unacceptable quality of measurements).
[h] Hip PDFF measurements were not available in 7 women (bilateral hip arthroplasty, $n = 3$; unacceptable quality of measurements, $n = 4$).

comparable. Again, in this study, no adjustments were made for fracture status or lumbar spine areal BMD values.

In contrast to the results of previous ^{1}H-MRS studies (Moorthi et al., 2015; Woods et al., 2018), we found no differences in PDFF measurements between eGFR categories, either at the lumbar spine or proximal hip. Postmenopausal women with eGFR ≥ 90 had lower lumbar spine PDFFs than other eGFR categories. However, adjusting for predetermined confounders – including age, diabetes, CCI, recent

Table 2
Association of imaging-based proton density fat fractions (PDFFs) with eGFR (treated according to pre-specify threshold and as continuous trait).

	eGFR treated as 3-level variable				eGFR treated as continuous variable	
	eGFR 30 to 59.9 ($n = 22$)	eGFR 60 to 89.9 ($n = 94$)	eGFR ≥ 90 % ($n = 83$)	p-Value	β [95%CI]	p-Value
Unadjusted model						
PDFF lumbar spine (%)	60.8 (56.8 to 64.8)	58.9 (57.0 to 60.9)	55.8 (53.8 to 57.9)	0.030	−1.1 (−1.8 to −0.2)	0.011
PDFF femoral neck (%)[a]	81.8 (78.2 to 85.4)	82.8 (81.0 to 84.5)	80.9 (79.0 to 82.7)	0.34	−0.09 (−0.82 to 0.65)	0.81
PDFF femoral diaphysis (%)[a]	80.6 (76.6 to 84.6)	81.2 (79.2 to 83.2)	79.9 (77.8 to 81.9)	0.64	0.03 (−0.78 to 0.85)	0.94
Model 1						
PDFF lumbar spine (%)	58.4 [54.3 to 62.5]	58.5 [56.6 to 60.4]	57.0 [54.9 to 59.1]	0.58	−0.3 (−1.2 to 0.6)	0.51
PDFF femoral neck (%)[a]	80.0 [76.3 to 83.6]	82.4 [80.7 to 84.2]	81.7 [79.8 to 83.6]	0.46	0.6 (−0.3 to 1.4)	0.17
PDFF femoral diaphysis (%)[a]	78.2 [74.1 to 82.3]	80.8 [78.8 to 82.7]	81.0 [78.9 to 83.0]	0.47	0.9 (0.01 to 1.8)	0.045
Model 2						
PDFF lumbar spine (%)	59.0 [54.1 to 63.9]	59.1 [56.4 to 61.7]	57.2 [54.4 to 60.1]	0.45	−0.4 (−1.5 to 0.6)	0.41
PDFF femoral neck (%)[a]	81.5 [77.7 to 85.4]	81.2 [79.0 to 83.4]	79.7 [77.3 to 82.1]	0.44	−0.4 (−0.9 to 0.8)	0.93
PDFF femoral diaphysis (%)[a]	80.3 [76.1 to 84.6]	80.2 [77.8 to 82.6]	79.4 [76.8 to 82.0]	0.83	0.2 (−0.7 to 1.2)	0.70
Model 3						
PDFF lumbar spine (%)	58.5 [53.4 to 63.5]	59.0 [56.3 to 61.7]	57.2 [54.3 to 60.0]	0.45	−0.5 (−1.5 to 0.5)	0.32
PDFF femoral neck (%)[a]	81.2 [77.2 to 85.3]	81.0 [78.8 to 83.2]	79.6 [77.2 to 82.0]	0.49	−0.3 (−1.1 to 0.6)	0.50
PDFF femoral diaphysis (%)[a]	80.5 [76.0 to 84.9]	80.2 [77.7 to 82.6]	79.4 [76.7 to 82.0]	0.82	0.1 (−0.9 to 1.1)	0.81
Model 4						
PDFF lumbar spine (%)	59.1 [54.1 to 64.1]	59.2 [56.5 to 61.9]	57.3 [54.4 to 60.1]	0.42	−0.4 (−1.5 to 0.6)	0.39
PDFF femoral neck (%)[a]	82.9 [78.9 to 86.8]	81.6 [79.4 to 83.8]	79.8 [77.4 to 82.1]	0.23	−0.2 (−1.0 to 0.7)	0.58
PDFF femoral diaphysis (%)[a]	80.9 [76.5 to 85.3]	80.4 [77.9 to 82.8]	79.4 [76.8 to 82.1]	0.75	0.1 (−0.9 to 1.1)	0.85

Values are mean [95 % CI] according to eGFR status, after adjustment for variables according to the model unless otherwise as indicated. β indicates regression coefficient per 10 % increase in eGFR.
Model 1: p-values were adjusted for age.
Model 2: p-values were adjusted for age, diabetes, Charlson Comorbidity Index, recent fragility fractures, aLM and lumbar spine BMD (or hip BMD).
Model 3: p-values were adjusted for age, diabetes, Charlson Comorbidity Index, recent fragility fractures, aLM, lumbar spine BMD (or hip BMD) and cFGF23.
Model 4: p-values were adjusted for age, diabetes, Charlson Comorbidity Index, recent fragility fractures, aLM, lumbar spine BMD (or hip BMD), SOST and cFGF23.
[a] Hip PDFF measurements were not available in 7 women (eGFR < 60 %, n = 1; eGFR 60–89.9 %, n = 5; eGFR ≥ 90 %, n = 1).

fragility fractures, aLM, and lumbar spine BMD – changed the magnitude of these associations.

Due to the design of the ADIMOS study, BMAT could only be evaluated up to stage 3 kidney disease. As such, designing a dedicated study to assess the impact of CKD on BMAT, including more advanced stages of CKD, would be of interest.

To date, only two studies have explored BMAT measurements in patients with advanced CKD treated with hemodialysis or renal transplantation (Hernandez et al., 2018b; Wang et al., 2022b). As these studies are beyond the scope of this article, they are not reported in detail. The first study compared histomorphometric BMAT parameters in patients with advanced CKD before kidney transplantation ($n = 29$) and age- and sex-matched controls (n = 29). The results showed that marrow adipocyte area/tissue area and marrow adipocyte volume/marrow volume were higher in patients with advanced CKD than in controls (Hernandez et al., 2018b). In another pilot study (Wang et al., 2022b), BMD, marrow adiposity index (MAI), VAT, and subcutaneous adipose tissue (SAT) were assessed in 15 hemodialysis patients (median age: 75 [66–82] years; 80 % male) using computed tomography (CT) scans. The main limitation of that study was the lack of a control group (non-CKD participants). Moreover, the sample size was small, and MRI is considered the gold standard for evaluating BMAT.

Interestingly, some data are available for animal models of CKD. In adenine-induced CKD rats, bone loss was found to be considerably higher and bone marrow adipocytes greater in number than in non-CKD control rats (Ni et al., 2019). In this model, serum PTH levels correlated with the levels of endothelial-to-mesenchymal transition (EndMT)-related proteins in BMAT. Endothelial-to-mesenchymal transition plays a key role in endothelial-to-adipocyte transition and subsequent BMAT elevation. In vitro treatment of cultured endothelial cells with PTH induced EndMT in a concentration- and time-dependent manner. Similarly, endothelial cells treated with PTH exhibited adipogenic potential following growth in an adipogenic culture medium, suggesting that the elevated PTH levels observed in CKD may increase adipogenesis by activating EndMT (Ni et al., 2019).

CKD-related osteoporosis remains poorly understood, and many factors, in addition to PTH, are involved in skeletal abnormalities in patients with CKD. In the ADIMOS-eGFR study, particular attention was paid to sclerostin and FGF23 since their expression by osteocytes is altered in CKD patients (Pelletier et al., 2013; Mazzaferro et al., 2018; Desbiens et al., 2022). In a study by Woods et al. (Woods et al., 2018), adjusting for sclerostin modestly reduced the relationship between vertebral marrow adiposity and kidney function, and the authors concluded that sclerostin may be a partial mediator. In our study, we did not obtain the same result. Elevated circulating FGF23 levels are also involved in the pathogenesis of CKD-mineral and bone disorders (CKD-MBD). We hypothesized that FGF23 mediates the relationship between marrow adiposity and kidney function. However, we failed to find any evidence of this mediator effect. Further studies are required to evaluate the association between FGF23 and BMAT.

4.1. Strengths and limitations

The strengths of this study lie in the fact that 1) serum measurements of kidney function and imaging-based PDFF assessments at both the lumbar spine and proximal hip were performed concurrently, 2) the study population was a large, well-characterized cohort of post-menopausal women with varying levels of kidney function, 3)

adjustments were made for key confounders, including aLM, and 4) the role of sclerostin and cFGF23 as potential mediators was investigated.

Our study had certain limitations. As the study was cross-sectional in design, it was not possible to evaluate the temporal association between eGFR and BMAT. Additionally, as the cohort was limited to post-menopausal women aged 50 years and older, our results may not apply to younger women or to men. Furthermore, we were unable to include a sufficient number of patients with eGFR <60, and especially patients with eGFR 30–45 ml/min/1.73 cm^2. Moreover, to quantify BMAT, we opted for chemical shift encoding-based water-fat imaging over spectral acquisitions because its implementation in routine MRI protocols is straightforward and because imaging-based PDFFs are highly correlated with 1H-MRS-based PDFFs (Paccou et al., 2023). Finally, this study did not include postmenopausal women with end-stage renal disease, i.e. stage 4 CKD (eGFR 15–29.9 ml/min/1.73 cm^2) or stage 5 CKD (eGFR < 15 ml/min/1.73 cm^2).

4.2. Conclusions

This study suggests that PDFFs are comparable across eGFR categories in postmenopausal women, regardless of BMAT measurement site. To confirm these findings, further studies designed specifically to analyze the impact of CKD on BMAT (including more advanced stages of kidney disease) are needed.

Supplementary data to this article can be found online at https://doi.org/10.1016/j.bonr.2023.101713.

CRediT authorship contribution statement

Sammy Badr: Conceptualization. **Anne Cotten:** Conceptualization. **Romuald Mentaverri:** Conceptualization. **Daniela Lombardo:** Project administration, Investigation. **Julien Labreuche:** Writing – review & editing, Formal analysis. **Claire Martin:** Writing – review & editing, Formal analysis. **Lucie Hénaut:** Writing – review & editing. **Bernard Cortet:** Writing – review & editing, Funding acquisition. **Julien Paccou:** Writing – review & editing, Writing – original draft, Conceptualization.

Declaration of competing interest

Anne Cotten has received an honorarium from Novartis. Bernard Cortet has received honoraria from Alexion, Amgen, Expanscience, Kyowa-Kirin, MSD, Novartis, Theramex, UCB and Viatris. Julien Paccou has received honoraria from Amgen, MSD, Eli Lilly, Kyowa-Kirin, Theramex and Pfizer. For the remaining authors, none were declared.

Data availability

The data supporting the findings of this study are available from the corresponding author upon reasonable request.

Acknowledgments

Funding: This work was supported by an unrestricted grant from MSD AVENIR.

Authors' roles: SB: Data curation, formal analysis, writing, reviewing, and editing. AC: Supervision, validation, writing (reviewing and editing). RM: Formal analysis, validation, writing (reviewing and editing). DL: Formal analysis, methodology, validation, writing (reviewing and editing). JL: Formal analysis, methodology, validation, writing (reviewing and editing). CM: Formal analysis, methodology, validation, writing (reviewing and editing). LH: Validation, writing (reviewing and editing). BC: Conceptualization, funding acquisition, methodology, supervision, validation, writing (reviewing and editing). JP: Conceptualization, methodology, project administration, visualization, writing (original draft).

References

Beekman, K.M., Duque, G., Corsi, A., Tencerova, M., Bisschop, P.H., Paccou, J., 2023. Osteoporosis and bone marrow adipose tissue. Curr. Osteoporos. Rep. 21, 45–55.
Courtalin, M., Bertheaume, N., Badr, S., During, A., Lombardo, D., Deken, V., Cortet, B., Clabaut, A., Paccou, J., 2023. Relationships between circulating sclerostin, bone marrow adiposity, other adipose deposits and lean mass in post-menopausal women. Int. J. Mol. Sci. 24, 5922.
Desbiens, L.C., Sidibé, A., Ung, R.V., Mac-Way, F., 2022. FGF23-klotho axis and fractures in patients without and with early CKD: a case-cohort analysis of CARTaGENE. J. Clin. Endocrinol. Metab. 107, e2502–e2512.
Fairfield, H., Falank, C., Harris, E., Demambro, V., McDonald, M., Pettit, J.A., et al., 2018. The skeletal cell-derived molecule sclerostin drives bone marrow adipogenesis. J. Cell. Physiol. 233, 1156–1167.
Hernandez, M.J., Dos Reis, L.M., Marques, I.D., Araujo, M.J., Truyts, C.A.M., Oliveira, I. B., et al., 2018a. The effect of vitamin D and zoledronic acid in bone marrow adiposity in kidney transplant patients: a post hoc analysis. PloS One 13, e0197994.
Hernandez, M.J., dos Reis, L.M., Marques, I.D., et al., 2018b. The effect of vitamin D and zoledronic acid in bone marrow adiposity in kidney transplant patients: a post hoc analysis. PloS One 13, e0197994.
Karampinos, D.C., Ruschke, S., Dieckmeyer, M., et al., 2018. Quantitative MRI and spectroscopy of bone marrow. J. Magn. Reson. Imaging 47, 332–353.
Lecka-Czernik, B., Baroi, S., Stechschulte, L.A., Chougule, A.S., 2018. Marrow fat-a new target to treat bone diseases? Curr. Osteoporos. Rep. 16, 123–129.
Li, Y., He, X., Olauson, H., Larsson, T.E., Lindgren, U., 2013. FGF23 affects the lineage fate determination of mesenchymal stem cells. Calcif. Tissue Int. 93, 556–564.
Li, J., Chen, X., Lu, L., Yu, X., 2020. The relationship between bone marrow adipose tissue and bone metabolism in postmenopausal osteoporosis. Cytokine Growth Factor Rev. 52, 88–98.
Mazzaferro, S., Cianciolo, G., De Pascalis, A., Guglielmo, C., Urena Torres, P.A., Bover, J., et al., 2018. Bone, inflammation and the bone marrow niche in chronic kidney disease: what do we know? Nephrol. Dial. Transplant. 33, 2092–2100.
Moorthi, R.N., Fadel, W., Eckert, G.J., Ponsler-Sipes, K., Moe, S.M., Lin, C., 2015. Bone marrow fat is increased in chronic kidney disease by magnetic resonance spectroscopy. Osteoporos. Int. 26, 1801–1807.
Ni, L.H., Tang, R.N., Yuan, C., Song, K.Y., Wang, L.T., Zhang, X.L., et al., 2019. Cinacalcet attenuated bone loss via inhibiting parathyroid hormone-induced endothelial-to-adipocyte transition in chronic kidney disease rats. Ann. Transl. Med. 7, 312.
Paccou, J., Hardouin, P., Cotten, A., Penel, G., Cortet, B., 2015. The role of bone marrow fat in skeletal health: usefulness and perspectives for clinicians. J. Clin. Endocrinol. Metab. 100, 3613–3621.
Paccou, J., Penel, G., Chauveau, C., Cortet, B., Hardouin, P., 2019. Marrow adiposity and bone: review of clinical implications. Bone 118, 8–15.
Paccou, J., Badr, S., Lombardo, D., Khizindar, H., Deken, V., Ruschke, S., Karampinos, D. C., Cotten, A., Cortet, B., 2023 Apr 5. Bone marrow adiposity and fragility fractures in postmenopausal women: the ADIMOS case-control study. J. Clin. Endocrinol. Metab., dgad195 https://doi.org/10.1210/clinem/dgad195. Online ahead of print. PMID: 37017011.
Pelletier, S., Dubourg, L., Carlier, M.C., Hadj-Aissa, A., Fouque, D., 2013. The relation between renal function and serum sclerostin in adult patients with CKD. Clin. J. Am. Soc. Nephrol. 8, 819–823.
Ruschke, S., Karampinos, D.C., 2022. Single-voxel short-TR multi-TI multi-TE STEAM MRS for water-fat relaxometry. Magn. Reson. Med. 87, 2587–2599.
Schwartz, A.V., Sigurdsson, S., Hue, T.F., Lang, T.F., Harris, T.B., Rosen, C.J., et al., 2013. Vertebral bone marrow fat associated with lower trabecular BMD and prevalent vertebral fracture in older adults. J. Clin. Endocrinol. Metab. 98, 2294–2300.
Wang, Y.P., Khelifi, N., Halleux, C., Ung, R.V., Samson, F., Gagnon, C., Mac-Way, F., 2022a. Bone marrow adiposity, bone mineral density and Wnt/β-catenin pathway inhibitors levels in hemodialysis patients. J. Bone Metab. 29, 113–122.
Wang, Y.P., Khelifi, N., Halleux, C., et al., 2022b. Bone marrow adiposity, bone mineral density and Wnt/β-catenin pathway inhibitors levels in hemodialysis patients. J. Bone Metab. 29, 113–122.
Woods, G.N., Ewing, S.K., Sigurdsson, S., Kado, D.M., Ix, J.H., Hue, T.F., Eiriksdottir, G., Xu, K., Gudnason, V., Lang, T.F., Vittinghoff, E., Harris, T.B., Rosen, C.J., Li, X., Schwartz, A.V., 2018. Chronic kidney disease is associated with greater bone marrow adiposity. J. Bone Miner. Res. 33, 2158–2164.
Woods, G., Ewing, S., Schafer, A., et al., 2022. Saturated and unsaturated bone marrow lipids have distinct effects on bone density and fracture risk in older adults. J. Bone Miner. Res. 37, 700–710.